The International Journal of Advanced Manufacturing Technology (2018) 95:4535–4546
https://doi.org/10.1007/s00170-017-1492-6

ORIGINAL ARTICLE

Weldability of marine grade AA 5052 aluminum alloy by underwater friction stir welding

S. Shanavas[1] · J. Edwin Raja Dhas[2] · N. Murugan[3]

Received: 20 February 2017 / Accepted: 14 December 2017 / Published online: 11 January 2018

Abstract
Friction stir welding (FSW) is a solid-state joining process producing high-quality welds with lower residual stresses and improved mechanical properties. Underwater FSW is a variant of FSW process which controls heat conduction and dissipation along the weld line improving the joint properties. The feasibility of underwater friction stir welding of AA 5052 H32 aluminum alloy to improve the joint performance than normal friction stir welding is addressed in this paper. The effects of tool rotational speed and welding speed on ultimate tensile strength by underwater and normal friction stir welding were analyzed and compared. It was observed that the tensile strength of underwater welded joints was higher than normal FSW joints except at 500 rpm. Maximum tensile strength of 208.9 MPa was obtained by underwater friction stir welding at 700 rpm tool rotational speed and welding speed of 65 mm/min. The optimum process parameters for achieving maximum tensile strength by normal FSW were compared with underwater FSW. The result showed that the ultimate tensile strength obtained by underwater FSW was about 2% greater than that of the normal FSW process. The joints with maximum tensile strength during underwater and normal welding fractured at the retreating side of the welded joint. Microstructural examination revealed that heat-affected region was not found in underwater welding. Microhardness was decreased slightly towards the stir zone. Fractography observation revealed that the welded joints exhibiting higher joint efficiency failed under ductile mode.

Keywords Aluminum alloy · Underwater friction stir welding · Tensile strength · Hardness · Fractography

1 Introduction

Marine grade aluminum alloys (5xxx series) are used as an alternative to steel in aerospace, marine, and automobile industries because of their light weight, good formability, good strength, and high corrosion resistance [1–3]. One of the most important characteristics of AA 5052-H32 aluminum alloy is its excellent corrosion resistance [2]. Fusion welding of those alloys is difficult [3]. Friction stir welding (FSW) is a solid-state joining process patented in 1991 by Thomas et al. [4] and being applied in various automotive industries due to its ability to produce high-quality joints [4–6]. Many factors influence the strength of FS welded joints. Tool geometry, tool rotational speed, welding speed, axial force, and tool tilt angle are the major factors used to control the heat generation and proper stirring action essential for joining the material effectively [7–15]. It is found that the tapered pin profile exhibited superior tensile properties compared to straight pin profile for AA7039 aluminum [9]. Researchers optimized FSW process parameters by regression modeling technique and soft computing technique [16–24]. Limited works were carried out on FSW of AA 5052-O aluminum alloy plates [25–27]. The effect of tool rotational speed on heat input during FSW of AA5052 aluminum alloy [26] was studied. The effect of tool rotational speed and tool tilt angle on the mechanical and metallurgical properties of the dissimilar friction stir butt joint between Al Alloy AA5052-H32 and HSLA steel [27] was investigated.

The strength of friction stir welded joints can be improved by controlling the level of temperature generated in FSW. This is achieved by immersing the work pieces in the liquid (water)

✉ J. Edwin Raja Dhas
edwinrajadhas@rediffmail.com

[1] Department of Mechanical Engineering, NIU, Kumaracoil, Tamil Nadu, India

[2] Department of Automobile Engineering, NIU, Kumaracoil, Tamil Nadu, India

[3] Department of Robotics and Automation Engineering, PSGCT, Coimbatore, Tamil Nadu, India

during the welding process [28–46]. Sakurada et al. [29] pioneered the usage of external water cooling for linear friction welding of 6061 aluminum alloys resulting in good bonding and weld strength. Sabari et al. [30] carried out an investigation on underwater FSW of AA 2519-T87 aluminum alloy and the study concluded that the process improved the strength of the joint by controlling the coarsening and dissolution of precipitates, resulted in narrow thermo-mechanically affected and heat-affected zones. Wang et al. [31] experimented underwater FSW to strengthen spray formed Al-Zn-Mg-Cu alloy. They compared the thermal cycle and property of underwater joint with that of normal FSW.

Heirani et al. [32] investigated the effects of process parameters on microstructure and mechanical behavior of underwater FS welded Al 5083 alloy. The result revealed that the hardness of the stir zone of water-cooled specimens was much higher than that of the specimens cooled in the air. Chen et al. [33] conducted a study on properties and microstructure of underwater FS welded ultra-high strength spray formed 7055 aluminum alloy joints. They reported that external water cooling improved the strength of joints, and the joint had a fine-grained microstructure than that of normal FS welded joint. Zhang et al. [34] developed a mathematical model and optimized underwater FSW process for 2219-T6 aluminum alloy. It was reported that the maximum strength obtained by underwater FSW was 6% higher than that obtained in normal FSW.

The effect of rotational speed on microstructure and mechanical properties of underwater FS welded 2219 aluminum alloy joints was observed by Zhang et al. [35]. It was found from the investigation that with increasing rotational speed, the hardness of the stir zone gradually increased due to the increase in dislocation density. The result also revealed that at lower rotational speed, the welded joint was fractured in the stir zone and, at higher rotational speeds, the hardness of the stir zone was increased and the fracture location was moved to the thermo-mechanically affected zone or heat-affected zone. Liu et al. [36] carried out an investigation on the effect of welding speed on microstructure and mechanical properties of underwater FS welded 2219 aluminum alloy. They reported that the joint welded at a lower welding speed was fractured in the heat-affected zone on the retreating side, while at higher welding speed, the joint was fractured in the thermo-mechanically affected zone on the advancing side.

Zhao et al. [37] studied the microstructural characterizations and mechanical properties of underwater FS welded dissimilar joint of aluminum and magnesium alloys. The result indicated that underwater welded joint had good mechanical

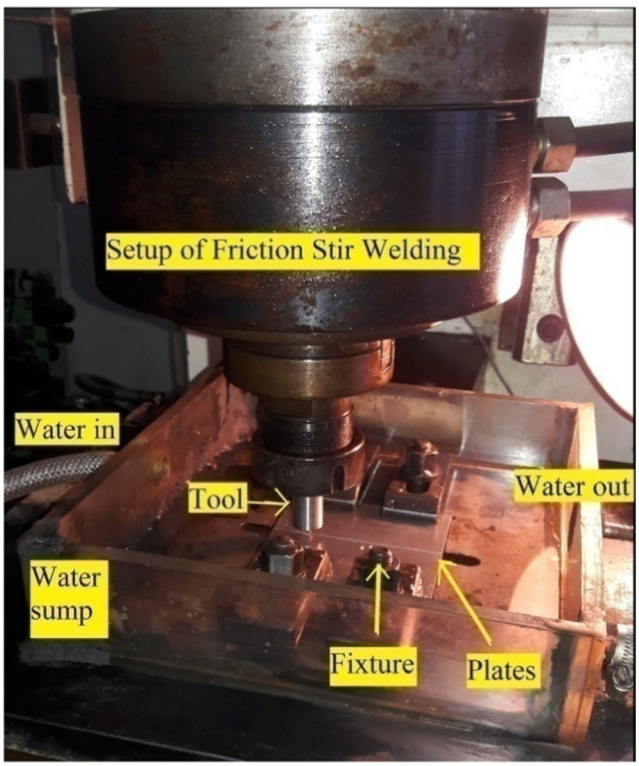

Fig. 1 Fixture setup used for underwater FSW

Fig. 2 Tapered FSW square pin profile tool

Table 1 FSW process parameters

Tool rotational speed (RPM)	Welding speed (mm/min)	Tool tilt angle (Degree)	Axial force (kN)
500	65	1.5	7
600	65	1.5	7
700	65	1.5	7
800	65	1.5	7
900	65	1.5	7
55	700	1.5	7
65	700	1.5	7
75	700	1.5	7
85	700	1.5	7

properties and the process produced recrystallization, forming complex intercalated flow patterns in the stir zone. Ramachandran et al. [38] developed a modified FSW process by water cooling to join aluminum alloy and high-strength low-alloy steel. The optimum process parameters for achieving maximum tensile strength by FSW were used to compare FSW with modified FSW and it was found that the ultimate tensile strength obtained by modified FSW was about 3% less than that of the normal FSW process. While comparing FSW with UFSW, the above literature shows that the potential welding parameters such as tool rotational speed and welding speed play a key role in determining the strength of the welded joints.

However, investigations using external cooling during FSW of high corrosion resistant marine grade aluminum alloy AA 5052 H32 have not been reported. In the present study, dry and wet FSW of AA 5052 aluminum alloy was performed. Effect of tool rotational speed and welding speed on ultimate tensile strength of FS welded AA 5052 aluminum alloy was studied and the results were compared with normal FSW. Tensile strength, microstructure, microhardness, and fracture features of the joints were compared.

2 Experimental procedure

For the present study, 6 mm cold rolled plates of high-strength aluminum-magnesium alloy AA 5052-H32 were used. The plates were cut and machined to 100 × 50 × 6 mm size, in which the 100 mm length was cut along the rolling direction and the adjoining surfaces were cleaned using acetone solution. The fixture designed for external cooling by water during the welding process is shown in Fig. 1. The welding direction was kept parallel to the rolling direction of the plate. The plates were welded in a single pass using tapered tool pin with a square profile having a taper angle of 10° and pin length of 5.7 mm (Fig. 2). The process was carried out in an electronically controlled semi-automatic FSW machine (make RV Machine Tools, India, and model FSW 5T-300-NC) with 50 kN maximum axial thrust force, 3000 rpm spindle speed, 5000 mm/min transverse speed, and ± 5° spindle tilt angle. The axial force can be set by setting the hydraulic pressure of oil (servo control). Considering the weld quality of AA 5052-H32 aluminum plates and tool wear rate, a non-consumable tool made of H13 steel with 54 HRC was selected [47–49] to fabricate the joints. The process parameters employed for the study are presented in Table 1. Photographs of the fabricated underwater friction stir welded joints are displayed in Figs. 3 and 4. The welding tool and the process parameters used both for underwater FSW and normal FSW were the same.

Samples were prepared from the welded plates by cutting using EDM at the center of the plate perpendicular to welding direction for metallographic analyses and tensile tests. For tensile test, three specimens were prepared from each welded plate as per ASTM–E8 standard [50]. Tensile tests were carried out by UTM, DAK-UTB 9103 with 100 kN capacity at a rate of loading of 2 mm/min. The samples extracted for microstructural examination were ground, then polished, and finally etched with modified Keller's etching solution [25]. Microstructures were observed by LEICA DM 2700 M metallurgical microscope. Microhardness measurement was carried out across the welded section at 1 mm interval by Vickers Microhardness Testing Machine (make Mitutoyo, Japan, and model HM113) using 50 gf load for 10 s holding time. Twenty-five spots were examined, and three readings were observed from each spot to minimize the error. The fractured surfaces of the tensile samples were examined by scanning electron microscope (SEM, Jeol JSM—6390LV/JED—2300) at different magnifications to analyze the fracture behavior of the joints.

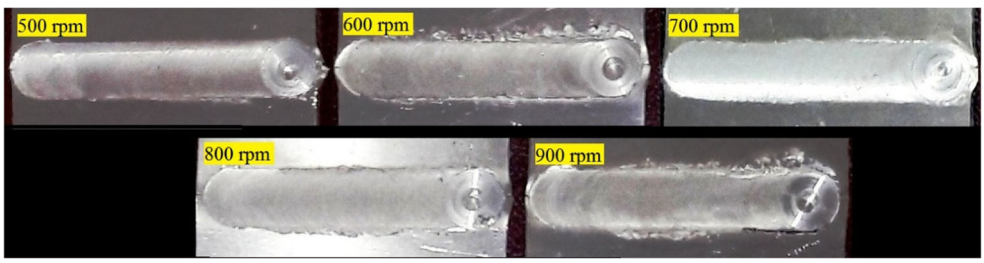

Fig. 3 Underwater friction stir welded plates at different tool rotational speeds

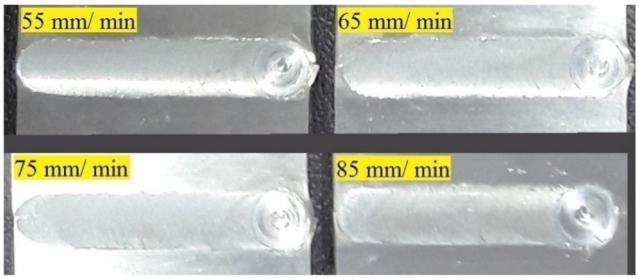

Fig. 4 Underwater friction stir welded plates at different welding speeds

3 Results and discussion

The effects of tool rotational speed and welding speed on mechanical properties are analyzed from the results obtained and detailed below.

3.1 Effect of tool rotational speed

The effect of tool rotational speed on tensile strength and yield strength of underwater friction stir welded plates was depicted in Fig. 5. From the figure, it is evident that both tensile strength and elongation initially increase with the increase in tool rotational speed and reach to a maximum value. Both tensile strength and % elongation decrease with the further increase in tool rotational speed [35, 38]. This may be due to the fact that heat input increases with the increase in tool rotational speed and reaches an optimum value at 700 rpm.

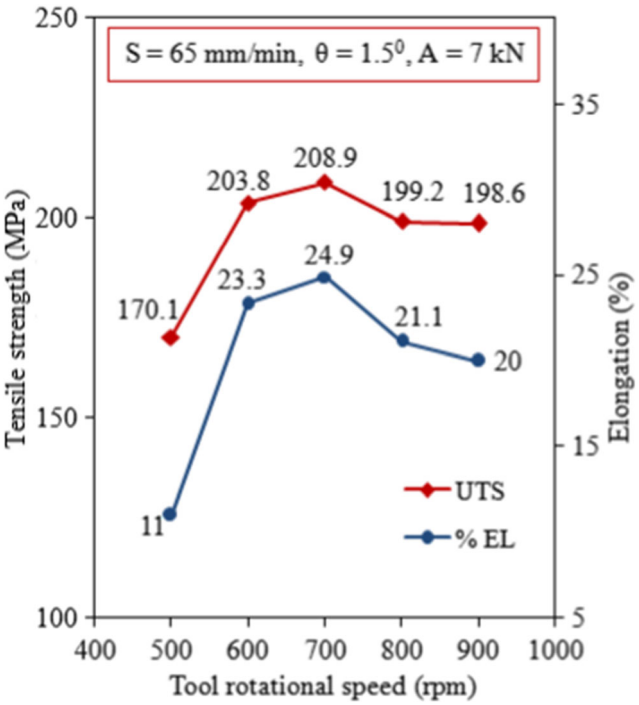

Fig. 5 Effect of tool rotational speed on tensile properties of underwater FS welded plates

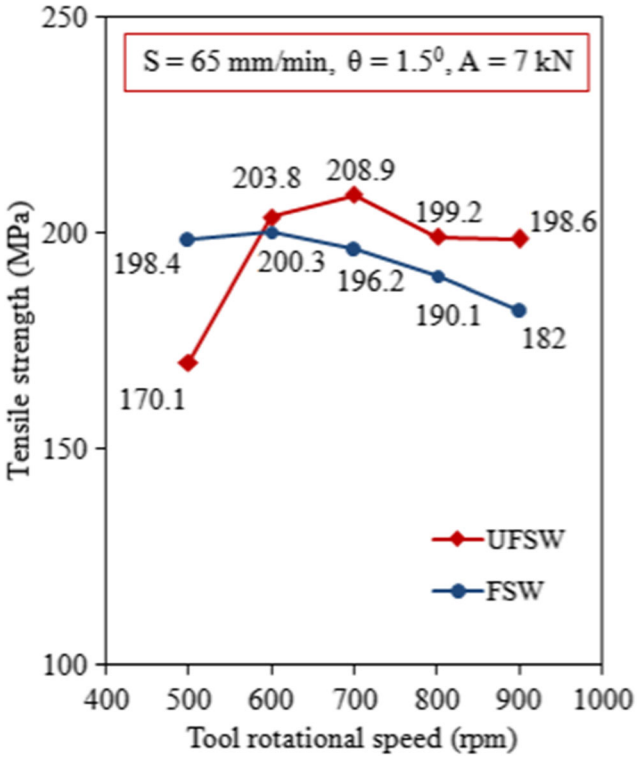

Fig. 6 Comparison of tensile strength of underwater FS welded plates at different tool rotational speeds with normal FS welded plates

At lower tool rotational speed, heat input is lower resulting poor consolidation of plastically deformed material resulting in lower strength. At higher tool rotational speed, the heat

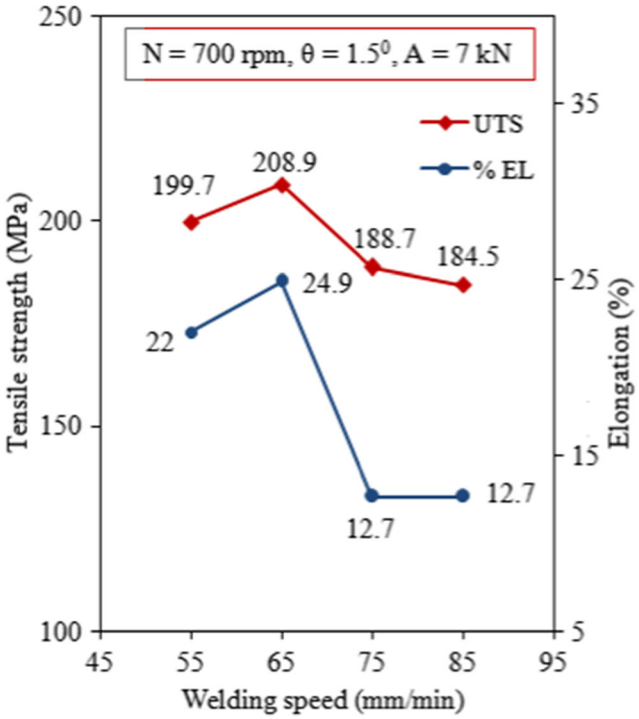

Fig. 7 Effect of welding speed on tensile properties of underwater FS welded plates

input is higher resulting in more turbulence in stir zone and poor consolidation of plasticized materials with lower tensile strength.

The tensile strength of underwater FS welded plates at different tool rotational speed is compared with that of normal FS welded plate and illustrated in Fig. 6. From the figure, it is clear that the tensile strength of the underwater FS welded plate is higher than that of normal FS welded plates except at 500 rpm. The higher strength may be due to the cooling effect resulting in finer grain size. At tool rotational speed of 500 rpm, the heat produced will not be sufficient to get good bonding resulting in reduced tensile strength.

3.2 Effect of welding speed

The effect of welding speed on mechanical properties of underwater FS welded plates is presented in Fig. 7. It is evident from the figure that initially tensile strength and % elongation increase slightly with the increase in welding speed and decrease with the further increase in welding speed [36]. When welding speed increases, the heat generated in FSW decreases. When the heat generated is not enough, the consolidation of the plasticized materials is not proper resulting in reduced tensile strength.

The tensile strength of underwater FS welded plates at different welding speeds is compared with that of normal FS welded plates and depicted in Fig. 8. It is found from the figure that the tensile strength of the underwater FS welded plate is higher than that of normal FS welded plates at all welding speeds. The higher strength may be due to the cooling effect resulting in finer grain size.

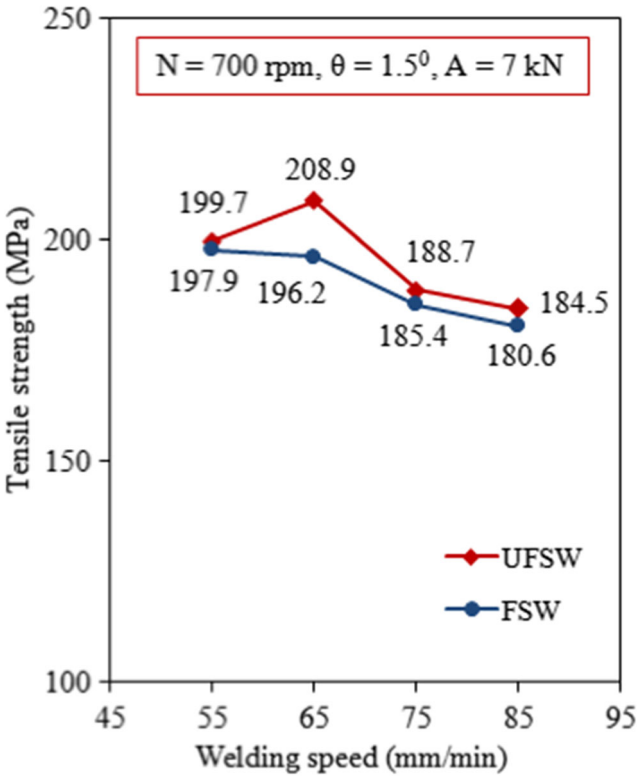

Fig. 8 Comparison of tensile strength of underwater FS welded plates at different welding speeds with normal FS welded plates

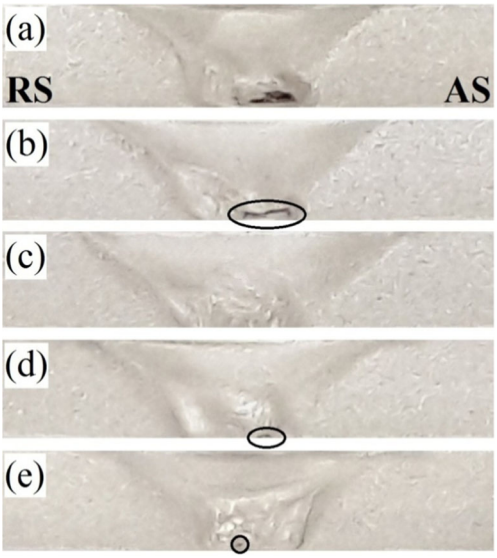

Fig. 9 Macrograph of the joints fabricated by UFSW at different tool rotational speed: **a** 500 rpm, **b** 600 rpm, **c** 700 rpm, **d** 800 rpm, and **e** 900 rpm

3.3 Macro and microstructural analysis

Macrographs of the joint fabricated at different tool rotational speed and welding speed are presented in Figs. 9 and 10, respectively. Lower rotational speed (< 700 rpm) or higher welding speed (> 65 mm/min) results in an insufficient vertical flow of material and poor weld metal consolidation, due to low heat generation, leading to tunneling defect at the root of the weld. Higher tool rotational speed (> 700 rpm) or lower welding speed (55 mm/min), resulted in an excess turbulence of plasticized metal and excess flash formation, due to excess

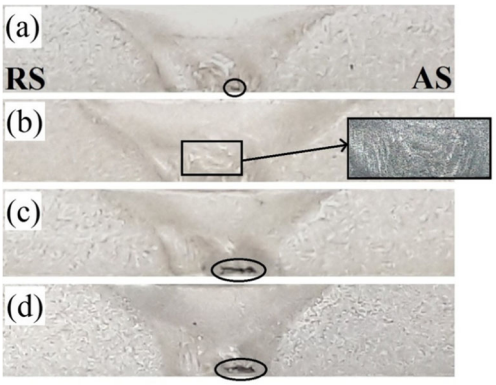

Fig. 10 Macrograph of the joints fabricated by UFSW at different welding speed: **a** 55 mm/min, **b** 65 mm/min, **c** 75 mm/min, and **d** 85 mm/min

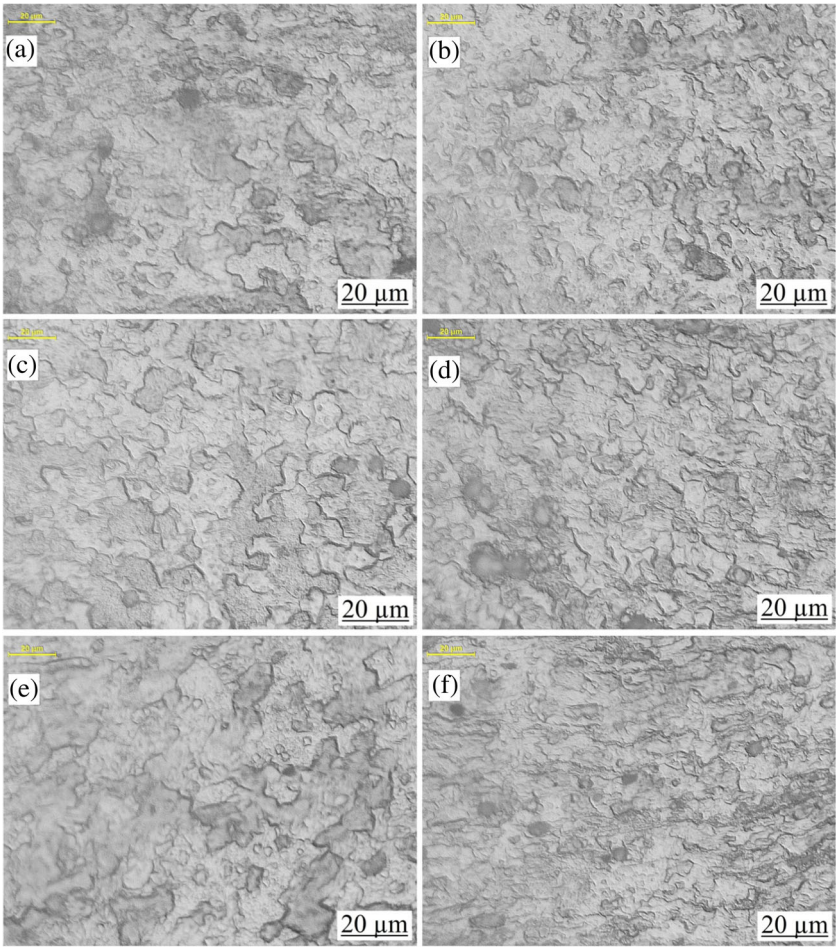

Fig. 11 Optical photomicrographs of the stir zone: **a** normal FS welded plates at 600 rpm, and underwater FS welded joints at different tool rotational speeds: **b** 500 rpm, **c** 600 rpm, **d** 700 rpm, **e** 800 rpm, and **f** 900 rpm

heat generation, lead to pin hole defect at the weld region. A defect-free weld is obtained at a rotational speed of 700 rpm and welding speed of 65 mm/min which is due to the optimum heat generation and proper consolidation of weld metal

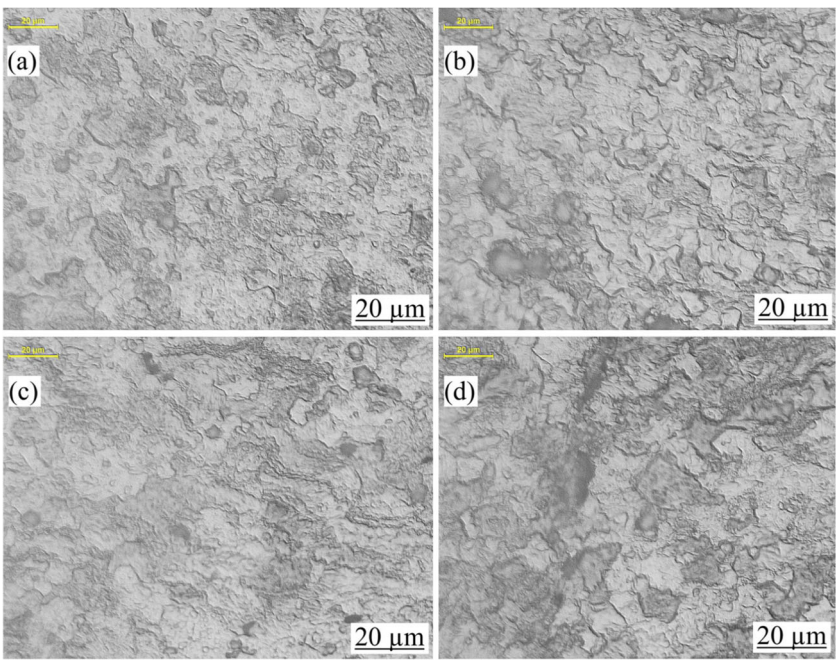

Fig. 12 Optical photomicrographs of the stir zone of underwater FS welded joints at different welding speeds: **a** 55 mm/min, **b** 65 mm/min, **c** 75 mm/min, and **d** 85 mm/min

occurred. An onion-ring structure is observed at the root of the weld.

Figure 11 shows the optical photomicrographs of the stir zone (SZ) of normal FS welded plate at 600 rpm and underwater FS welded plates at different tool rotational speeds. Figure 12 shows the optical photomicrographs of the stir zone of underwater FS welded plates at different welding speeds. The plates welded at rotational speed of 600 rpm and welding speed of 65 mm/min were considered for the study. Equiaxed grain structure is observed at SZ of the welded plates joined by both processes. Finer equiaxed grains are found at SZ of the welded plates by underwater FSW process than normal FSW process. Water cooling enhances smooth material flow at low/optimum heat input which results in better recrystallization of material at the stir zone. It also helps to maintain a uniform heat input along the weld line. The heat-affected region (HAZ) is the weaker region where crack propagates in high-strength welded joints. The absence of this region is found in underwater FS welded plates which may be due to faster heat dissipation during water cooling. For these reasons, the plates welded by underwater FSW process showed a high resistance to fracture compared to normal FSW process.

EBSD images of stir zone of normal FS welded plate at 600 rpm and underwater FS welded plates at different rotational speed and welding speed are presented in Fig. 13 and Fig. 14, respectively. The stir zone exhibits equiaxed grains as a result of dynamic recrystallization during FSW. The average grain size in the stir zone of joints welded by normal FSW and underwater FSW at tool rotational speed of 600 rpm and welding speed of 65 mm/min is 6.9 and 5.3 μm, respectively. More refinement of grain in the stir zone of joints welded by underwater FSW is due to decrease is heat input. The average grain size at rotational speeds of 500, 600, 700, 800, and 900 rpm is 5.9, 5.3, 5.1, 6.9, and 8.9 μm, respectively, and that of welding speeds of 55, 65, 75, and 85 mm/min are 7.1, 5.1, 6.1, and 6.4 μm, respectively. The grain refinement at stir zone is mainly due to heat input and strain rate. The increase in tool rotational speed or decrease in welding speed results in an increase in both heat input and the strain rate at stir zone, whereas the decrease in rotational speed or increase in welding speed results in a decrease in both heat input and the strain rate at stir zone.

Generally, the increase in strain rate or decrease in heat input leads to grain refinement, while the increase in heat input or decrease in strain rate tends to increase grain size [35, 36]. That is, the increase or decrease in grain size depends on both factors. In underwater FSW process, a portion of the heat generated is carried away by the surrounding water. At higher rotational speed or lower welding speed, even after carrying away a portion of the heat generated by the surrounding water, the heat input is very high. But at lower rotational speed or higher welding speed, the generated heat is very less even

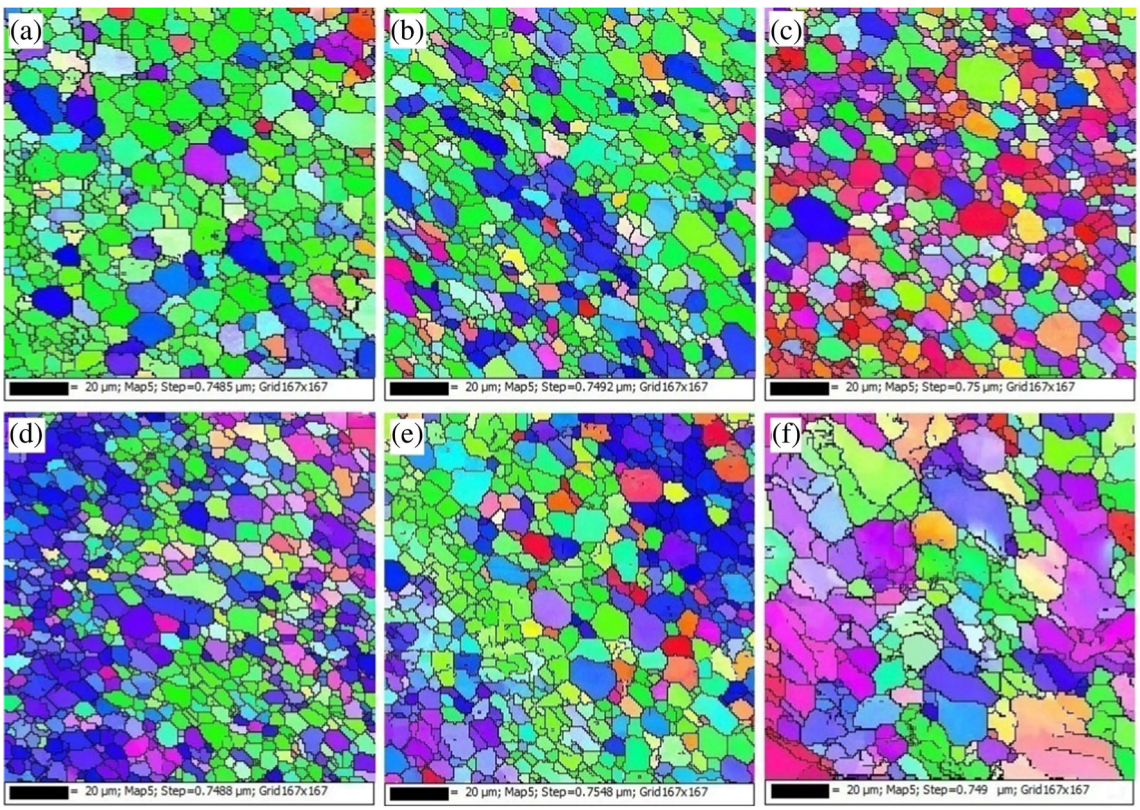

Fig. 13 EBSD (IPF map) image of the stir zone: **a** normal FS welded plates at 600 rpm, and underwater FS welded joints at different tool rotational speeds: **b** 500 rpm, **c** 600 rpm, **d** 700 rpm, **e** 800 rpm, and **f** 900 rpm

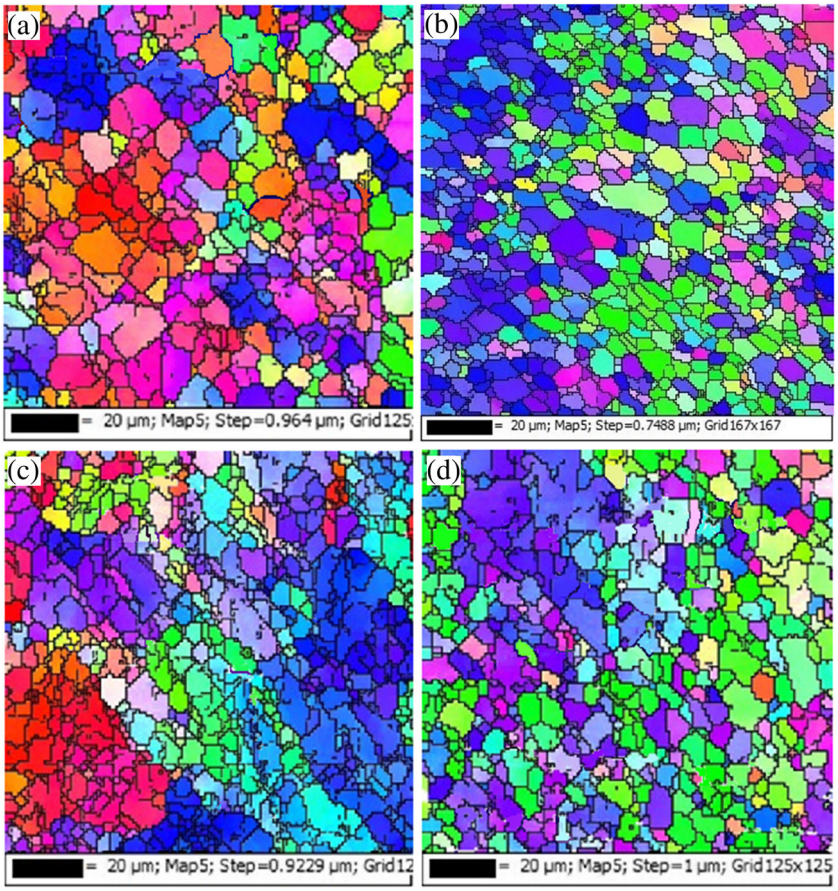

Fig. 14 EBSD (IPF map) image of the stir zone of underwater FS welded joints at different welding speeds: **a** 55 mm/min, **b** 65 mm/min, **c** 75 mm/min, and **d** 85 mm/min

though some of the heat is carried away by the surrounding water. But sufficient heat input is necessary for dynamic recrystallization. Therefore, it seems that strain rate controls the grain size at lower rotational speed or higher welding speed; whereas heat input controls the grain size at higher rotational speed or lower welding speed results in increase in grain size.

Microhardness distribution on the transverse cross-section of the normal and underwater FS welded joints at welding speed of 65 mm/min and rotational speed of 600 rpm is shown in Fig. 15. The average hardness observed on the normal and underwater FS welded joints is found to be lower than that of the base metal (67 Hv). The base material AA 5052-H32 aluminum is strain hardened by cold working. The average hardness observed on the normal FS welded joint (60 Hv) is slightly less compared to that of the underwater FS welded joint (61 Hv). The equiaxed grain size is smaller in the stir zone of underwater FSW joint, which would increase the hardness according to Hall-Petch relation. The hardness improved may be also due to the increase in dislocation density. The hardness is decreased at the stir zone. The decrease in hardness towards the stir zone is due to the recovery and recrystallization occurred in the stir zone during the welding process. The same effect has been reported for cold worked (strain hardened) aluminum alloy [4]. There is no significant

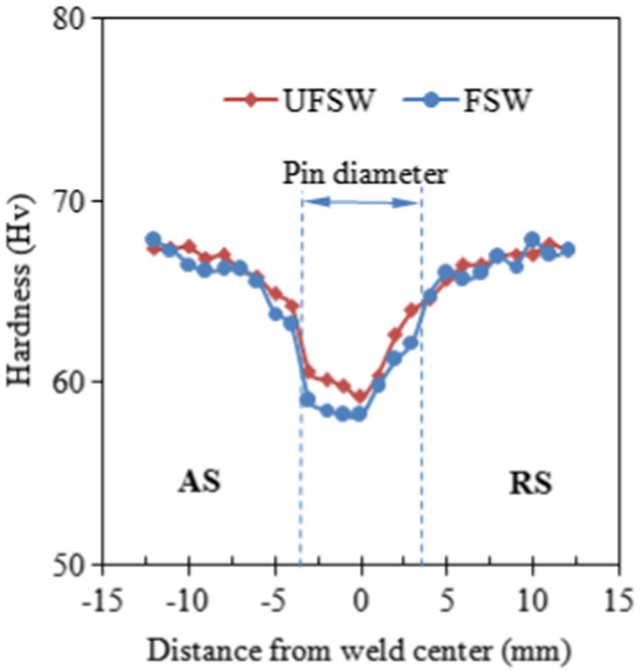

Fig. 15 Microhardness distribution along the cross section perpendicular to the welding direction at welding speed of 65 mm/min and rotational speed of 600 rpm

variation in hardness in the advancing side (AS) and the retreating side (RS) of welded joints.

3.4 Fractography

Location of fracture in the tensile samples at different tool rotational speeds and welding speeds is shown in Fig. 16. During the tensile test, the welded joints produced at lower rotational speed (500 rpm) and at higher welding speeds (75 and 85 mm/min) exhibit a lower joint efficiency (< 90) compared to other welded joints considered for the study. It is found that these joints are fractured at the stir zone of the joint due to the low frictional heat generated. At lower heat generation, the layer-by-layer material consolidation occurred leads to poor bonding at stir zone resulting in reduced strength of the joint. Since the welded joints are highly heterogeneous with weld nugget at the center, TMAZ, HAZ, and base metal on either side, the joints are failed at the weaker region.

The welded joints produced at higher rotational speeds (800 and 900 rpm) and at lower welding speed (55 mm/min) exhibit a joint efficiency of 92%. These joints are fractured at the advancing side of the welded joints, indicating that the tensile strength on the advancing side is lower than that of the retreating side. Good bonding at the stir zone due to optimum heat generation and strain rate at the stir zone makes stir zone stronger and failure occurs on the either sides of the stir zone. Generally, the heat generation and material consolidation are more at the advancing side compared to the retreating side of the welded joints. The higher rotational speed and lower welding speed lead to higher heat generation at advancing side resulting in poor bonding at advancing side.

The welded joints produced at a rotational speed of 600 and 700 rpm with a welding speed of 65 mm/min exhibit a sound joint having weld joint efficiencies of 94 and 96%, respectively, and those joints are fractured at the retreating side because of the better consolidation of the material at the stir zone and at the advancing side of the welded joints.

Figure 17 shows SEM images of the tensile fractured surface of the base metal and underwater FS welded joints at different rotational speeds. The fractured surface was perpendicular to the tensile axis. The fractured surface of the base metal and the welded joints produced at a rotational speed of 600 and 700 rpm consists of small dimples, indicating a decrease of plastic deformation level during the tensile test. The fractography reveals that the joints failed under ductile mode. These joints exhibit higher joint efficiency (> 94%). However, dimples were found both small and large size in the fractured surface of the welded joints produced at a higher rotational speed of 800 and 900 rpm, indicating that an extensive plastic deformation occurred during the tensile test. The fracture mechanism is close to quasi-cleavage fracture. These joints exhibit a higher joint efficiency of around 92%. The large dimples reflect the distorted and grown grains; in turn, the small equiaxed dimples characterize recrystallized grain structure. At high magnification, the fractured surface of the welded joint produced at a lower rotational speed of 500 rpm reveals extensive plastic deformation with a large number of smooth planar facets. This joint exhibits lower joint efficiency compared to other joints (< 90%). Higher magnification of the fractured surface of the welded joint produced at rotational speed of 700 rpm shows clearly a very dense grouping of very small dimples around large dimples. This joint exhibits the maximum joint efficiency of 96%. There is no evidence of either grain boundary facets or inclusion at the surface.

Figure 18 shows SEM images of the tensile fractured surface of the underwater FS welded joints at different welding speeds. The fractured surface of the welded joint produced at lower welding speed of 55 mm/min consists of dimples of both small and large size in the fractured surface, indicating an extensive plastic deformation occurred during the tensile test. The fracture mechanism is close to quasi-cleavage fracture. This joint exhibits a higher joint efficiency of 92%. The

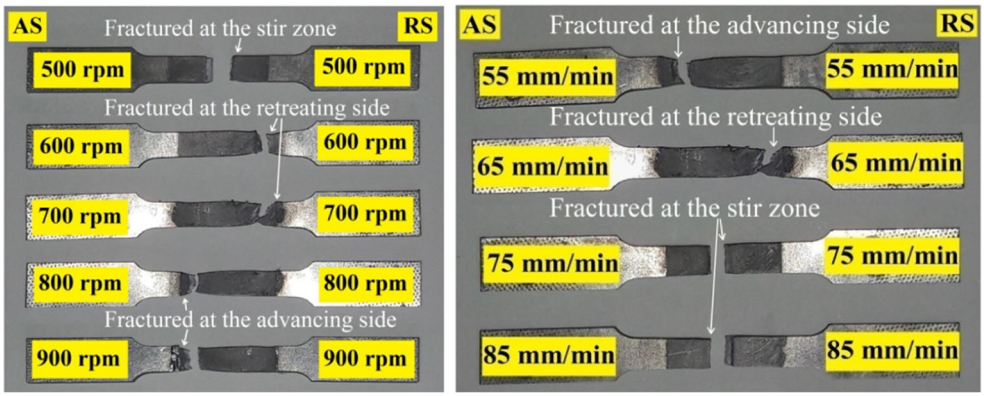

Fig. 16 Fractured tensile specimens showing the location of fracture

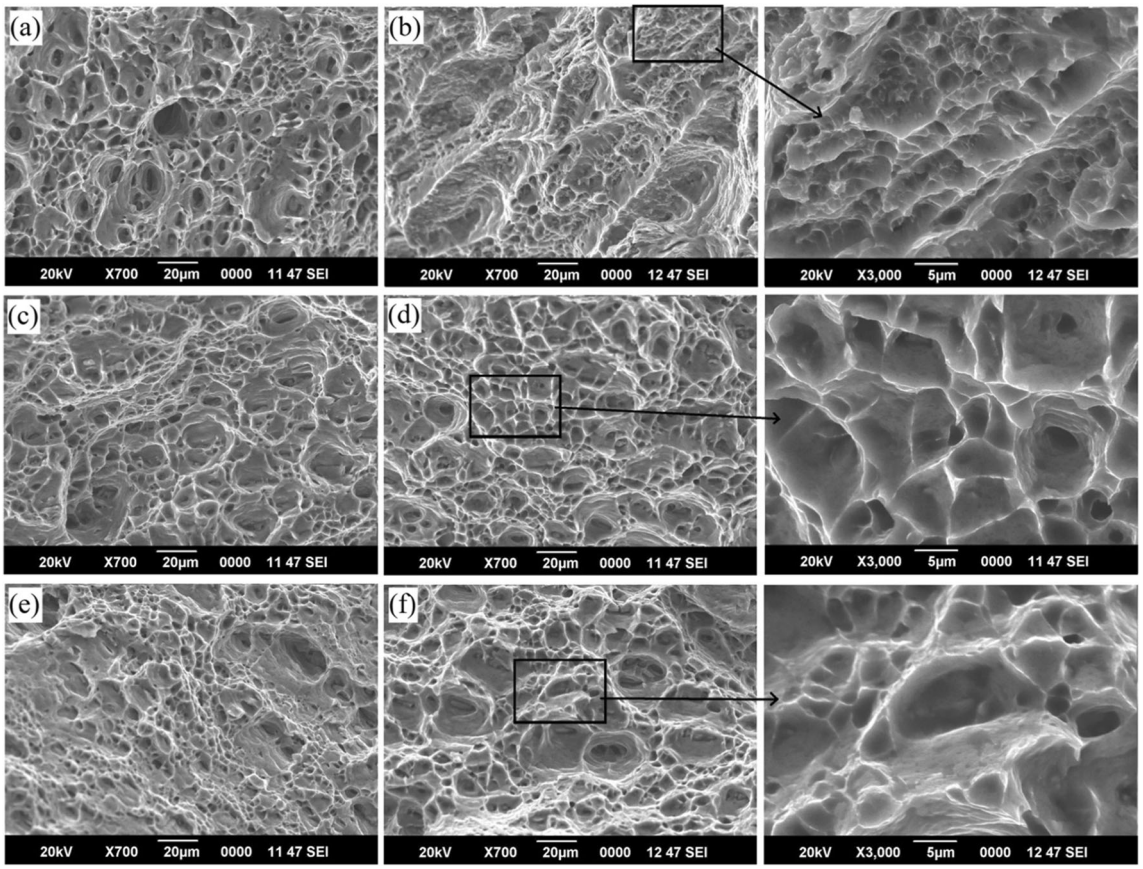

Fig. 17 Fractured surface of **a** base metal, and underwater FS welded joints at different tool rotational speeds: **b** 500 rpm, **c** 600 rpm, **d** 700 rpm, **e** 800 rpm, and **f** 900 rpm

fractured surface of the welded joint produced at higher welding speeds of 75 and 85 mm/min reveals extensive plastic deformation with a large number of smooth planar facets. These joints exhibit lower joint efficiency compared to other joints (< 90%). The result shows that the fractured surface of the joints exhibiting higher joint efficiency consists of dense and small dimples and joints fail by ductile mode, whereas the fractured surface of the joints exhibit lower joint efficiency

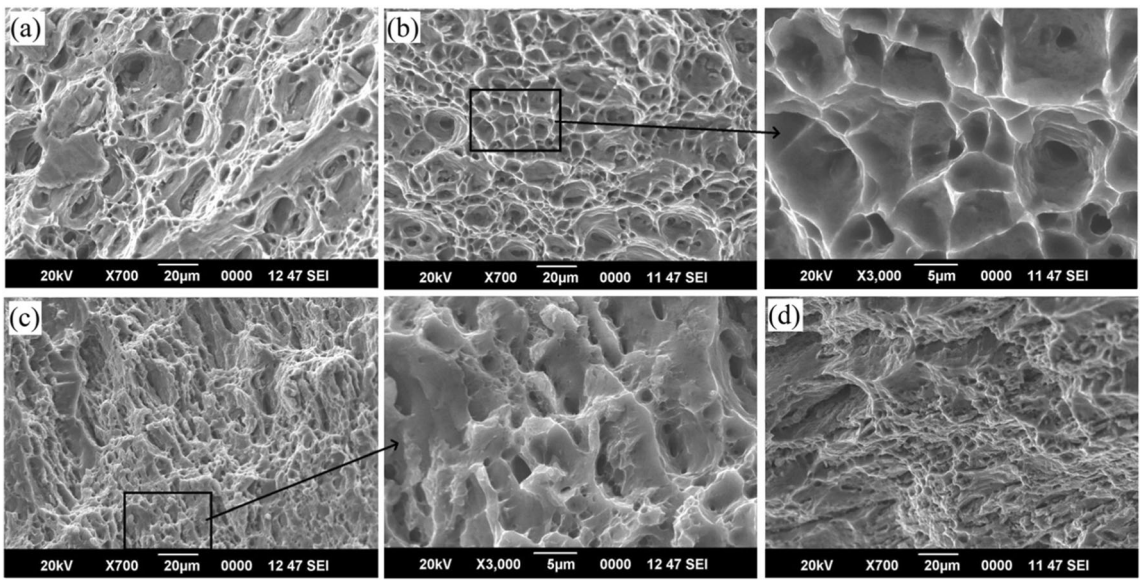

Fig. 18 Fractured surface of underwater FS welded joints at different welding speeds: **a** 55 mm/min, **b** 65 mm/min, **c** 75 mm/min, and **d** 85 mm/min

consists of a large number of smooth planar facets and joints fail by plastic deformation.

4 Conclusions

The following conclusions are drawn from the experimental investigation on underwater friction stir welding of a marine grade AA 5052-H32 aluminum alloy.

1) Tensile strength increased with the increase in tool rotational speed reaching a maximum and it decreased with the further increase in tool rotational speed. The tensile strength of underwater welded joints was higher than normal FS welded joints except at 500 rpm.
2) The joints having maximum tensile strength produced by both underwater and normal FSW were fractured at the retreating side of the welded joint.
3) The maximum tensile strength of 208.9 MPa of the joints produced by underwater FSW was obtained at tool rotational speed of 700 rpm, whereas the maximum tensile strength of 200.3 MPa of the joints produced by normal friction stir welding was obtained at tool rotational speed of 600 rpm. The other parameters such as the welding speed, axial load, and tool tilt angle were kept constant at 65 mm/min, 7 kN, and 1.5°, respectively.
4) The optimum process parameters for achieving maximum tensile strength by normal FSW is used to compare it with underwater FSW and it was found that the ultimate tensile strength obtained by underwater FSW is about 2% greater than that of the normal FSW process.
5) The absence of HAZ region was found in underwater FSW process which might be due to faster heat dissipation by water cooling. Finer equiaxed grains were found at SZ of the welded plates by underwater FSW process than normal FSW process.
6) The fractured surface of the joints exhibiting higher joint efficiency consisted of dense and small dimples and joints failed by ductile mode, whereas the fractured surface of the joints exhibiting lower joint efficiency consisted of a large number of smooth planar facets and joints failed by plastic deformation.

Acknowledgements The authors are grateful to the Department of Mechanical Engineering, Coimbatore Institute of Technology, India, for extending the facilities to carry out the investigations.

References

1. Chen J, Yuan X, Hu Z, Sun C, Zhang Y, Zhang Y (2016) Microstructure and mechanical properties of resistance-spot-welded joints for A5052 aluminum alloy and DP 600 steel. Mater Charact 120:45–52. https://doi.org/10.1016/j.matchar.2016.08.015
2. Zhang R, Knight SP, Holtz RL, Goswami R, Davies CHJ, Birbilis N (2016) A survey of sensitization in 5xxx series aluminum alloys. Corros Sci 72(2):144–159. https://doi.org/10.5006/1787
3. Zhitong Chen, Shengxi Li, Kaimiao Liu, Lloyd H. Hihara arXiv: 1511.04990 (2015) A study on the mechanical property and corrosion sensitivity of an AA5086 friction stir welded joint. arXiv e-print (arXiv:1511.04990)
4. Mishra RS, Ma ZY (2005) Friction sir welding and processing. Material Sci Engineering R 50(1-2):1–78. https://doi.org/10.1016/j.mser.2005.07.001
5. Grimm A, Schulze S, Silva A, Gobel G, Standfuss J, Brenner B, Beyer E, Fussel U (2015) Friction stir welding of light metals for industrial applications. Materials Today: Proceedings 2S:169–178. https://doi.org/10.1016/j.matpr.2015.05.007
6. Gibson BT, Lammlein DH, Prater TJ, Longhurst WR, Cox CD, Ballun MC, Dharmaraj KJ, Cook GE, Stauss AM (2014) Friction stir welding: process, automation, and control. J Manufacturing Process 16(1):56–73. https://doi.org/10.1016/j.jmapro.2013.04.002
7. Saravanan V, Rajakumar S, Banerjee N, Amuthakkannan R (2016) Effect of shoulder diameter to pin diameter ratio on microstructure and mechanical properties of dissimilar friction stir welded AA2024-T6 and AA7075-T6 aluminum alloy joints. Int J Adv Manuf Technol 87(9-12):3637–3645. https://doi.org/10.1007/s00170-016-8695-0
8. Elangovan K, Balasubramanian V (2008) Influence of tool pin profile and welding speed on the formation of friction stir processing zone in AA2219 aluminium alloy. J Mater Process Technol 200(1-3):163–175. https://doi.org/10.1016/j.jmatprotec.2007.09.019
9. Ugender S, Kumar A, Somi Reddy A (2014) Experimental investigation of tool geometry on mechanical properties of friction stir welding of AA 2014 aluminium alloy. Procedia Materials Sci 5: 824–831. https://doi.org/10.1016/j.mspro.2014.07.334
10. Bayazid SM, Farhangi GA (2015) Effect of pin profile on defects of friction stir welded 7075 aluminum alloy. Procedia Materials Sci 11:12–16. https://doi.org/10.1016/j.mspro.2015.11.013
11. Yue Y, Zhou Z, Ji S, Zhang J, Li Z (2017) Effect of welding speed on joint feature and mechanical properties of friction stir lap welding assisted by external stationary shoulders. Int J Adv Manuf Technol 89(5-8):1691–1698. https://doi.org/10.1007/s00170-016-9240-x
12. Gadakh VS, Adepu K (2013) Heat generation model for taper cylindrical pin profile in FSW. J Materials Res Technol 2(4):370–375. https://doi.org/10.1016/j.jmrt.2013.10.003
13. Liu H, Zhao Y, Hu Y, Chen S, Lin Z (2015) Microstructural characteristics and mechanical properties of friction stir lap welding joint of alclad 7B04-T74 aluminum alloy. Int J Adv Manuf Technol 78(9-12):1415–1425. https://doi.org/10.1007/s00170-014-6718-2
14. Zhang Z, Wu Q (2015) Analytical and numerical studies of fatigue stresses in friction stir welding. Int J Adv Manuf Technol 78(9-12): 1371–1380. https://doi.org/10.1007/s00170-014-6749-8
15. Amini S, Amiri MR (2015) Pin axis effects on forces in friction stir welding process. Int J Adv Manuf Technol 78(9-12):1795–1801. https://doi.org/10.1007/s00170-015-6785-z
16. Rajakumar S, Balasubramanian V (2012) Establishing relationships between mechanical properties of aluminium alloys and optimised friction stir welding process parameters. Mater Des 40:17–35. https://doi.org/10.1016/j.matdes.2012.02.054
17. Venkateswarlu D, Mandal NR, Mahapatra MM, Harsh SP (2013) Tool design effects for FSW of AA7039. Weld J 92:41–47
18. Elatharasan G, Senthil Kumar VS (2013) An experimental analysis and optimization of process parameter on friction stir welding of AA 6061-T6 aluminium alloy using RSM. Procedia Engineering 64:1227–1234. https://doi.org/10.1016/j.proeng.2013.09.202

19. Kadaganch R, Gankidi MR, Gokhale H (2015) Optimization of process parameters of aluminum alloy AA 2014-T6 friction stir welds by response surface methodology. Defence Technol 11(3): 209–219. https://doi.org/10.1016/j.dt.2015.03.003
20. Lakshminarayanan AK, Balasubramanian V (2009) Comparison of RSM with ANN in predicting tensile strength of friction stir welded AA7039 aluminium alloy joints. Trans Nonferrous Metals Soc China 19(1):9–18. https://doi.org/10.1016/S1003-6326(08)60221-6
21. Jayaraman M, Sivasubramanian R, Balasubramanian V, Lakshminarayanan AK (2009) Application of RSM and ANN to predict the tensile strength of friction stir welded A319 cast aluminum alloy. Int J Manuf Res 4(3):306–323. https://doi.org/10.1504/IJMR.2009.026576
22. Palanivel R, Laubscher RF, Dinaharan I, Murugan N (2016) Tensile strength prediction of dissimilar friction stir-welded AA6351–AA5083 using artificial neural network technique. J Braz Soc Mech Sci Eng 38(6):1647–1657. https://doi.org/10.1007/s40430-015-0483-5
23. Ghetiya ND, Patel KM (2014) Prediction of tensile strength in friction stir welded aluminium alloy using artificial neural network. Procedia Technol 14:274–281. https://doi.org/10.1016/j.protcy.2014.08.036
24. Okuyucu H, Kurt A, Arcaklioglu E (2007) Artificial neural network application to the friction stir welding of aluminum plates. Mater Des 28(1):78–84. https://doi.org/10.1016/j.matdes.2005.06.003
25. Moshwan R, Yusof F, Hassan MA, Rahmat SM (2015) Effect of tool rotational speed on force generation, microstructure and mechanical properties of friction stir welded AA 5052-O alloy. Mater Des 66:118–128. https://doi.org/10.1016/j.matdes.2014.10.043
26. Kwon Y-J, Shim S-B, Park D-H (2009) Friction stir welding of 5052 aluminum alloy plates. Trans Nonferrous Metals Soc China 19:23–27. https://doi.org/10.1016/S1003-6326(10)60239-7
27. Ramachandran KK, Murugan N, Shashi kumar S (2015) Friction stir welding of aluminum alloy AA5052 and HSLA steel. Weld J 94:291–300
28. Shanavas S, Edwin Raja Dhas J (2017) Modeling and analysis of friction stir welding and underwater friction stir welding of aluminium alloy: a review. Appl Mech Mater 867:127–133. https://doi.org/10.4028/www.scientific.net/AMM.867.127
29. Sarukada D, Katoh K, Tokisue H (2002) Underwater friction welding of 6061 aluminum alloy. J Japan Institute Light Metals 52:2–6. https://doi.org/10.2464/jilm.52.2
30. Sabari Sree S, Malarvizhi S, Balasubramanian V, Madusudahan Reddy G (2016) Experimental and numerical investigation on under-water friction stir welding of armour grade AA2519-T87 aluminium alloy. Defence Technol 12(4):324–333. https://doi.org/10.1016/j.dt.2016.02.003
31. Wang Q, Zhao Z, Zhao Y, Yan K, Liu C, Zhang H (2016) The strengthening mechanism of spray forming Al-Zn-Mg-Cu alloy by underwater friction stir welding. Mater Des 102:91–99. https://doi.org/10.1016/j.matdes.2016.04.036
32. Heirani F, Abbasi A, Ardestani M (2017) Effects of processing parameters on microstructure and mechanical behaviors of underwater friction stir welding of Al5083 alloy. J Manuf Process 25:77–84. https://doi.org/10.1016/j.jmapro.2016.11.002
33. Chen H, Zhao Y, Wang Q, Yan K (2014) Microstructure and mechanical properties of spray formed 7055 aluminum alloy by underwater friction stir welding. Mater Des 56:725–730. https://doi.org/10.1016/j.matdes.2013.11.071
34. Zhang H, Liu H (2013) Mathematical model and optimization for underwater friction stir welding of a heat-treatable aluminum alloy. Mater Des 45:206–211. https://doi.org/10.1016/j.matdes.2012.09.022
35. Zhang HJ, Liu HJ, Yu L (2011) Microstructure and mechanical properties as a function of rotation speed in underwater friction stir welded aluminum alloy joints. Mater Des 32(8-9):4402–4407. https://doi.org/10.1016/j.matdes.2011.03.073
36. Liu HJ, Zhang HJ, Yu L (2011) Effect of welding speed on microstructures and mechanical properties of underwater friction stir welded 2219 aluminum alloy. Mater Des 32(3):1548–1553. https://doi.org/10.1016/j.matdes.2010.09.032
37. Zhao Y, Lu Z, Yan K, Huang L (2015) Microstructural characterizations and mechanical properties in underwater friction stir welding of aluminum and magnesium dissimilar alloys. Mater Des 65:675–681. https://doi.org/10.1016/j.matdes.2014.09.046
38. Ramachandran KK, Murugan N, Shashi Kumar S (2015) Study on dissimilar butt joining of aluminum alloy, AA5052 and high strength low alloy steel through a modified FSW process. Mater Sci Forum 830:278–281. https://doi.org/10.4028/www.scientific.net/MSF.830-831.278
39. Sree Sabari S, Malarvizhi S, Balasubramanian V (2016) Characteristics of FSW and UWFSW joints of AA2519-T87 aluminium alloy: effect of tool rotation speed. J Manuf Process 22: 278–289. https://doi.org/10.1016/j.jmapro.2016.03.014
40. Zhao Y, Jiang S, Yang S, Lu Z, Yan K (2016) Influence of cooling conditions on joint properties and microstructures of aluminum and magnesium dissimilar alloys by friction stir welding. Int J Adv Manuf Technol 83(1-4):673–679. https://doi.org/10.1007/s00170-015-7624-y
41. Wang BB, Chen FF, Liu F, Wang WG, Xue P, Ma ZY (2017) Enhanced Mechanical Properties of Friction Stir Welded 5083Al-H19 Joints with Additional Water Cooling. Journal of Materials Science & Technology 33:1009-1014. https://doi.org/10.1016/j.jmst.2017.01.016
42. Sree Sabari S, Malarvizhi S, Balasubramanian V (2016) Influences of tool traverse speed on tensile properties of air cooled and water cooled friction stir welded AA2519-T87 aluminium alloy joints. J Mater Process Technol 237:286–300. https://doi.org/10.1016/j.jmatprotec.2016.06.015
43. Zhang H-j, Liu H-j, Yu L (2013) Thermal modeling of underwater friction stir welding of high strength aluminum alloy. Trans Nonferrous Metals Soc China 23(4):1114–1122. https://doi.org/10.1016/S1003-6326(13)62573-X
44. Zhang J, Shen Y, Yao X, Xu H, Li B (2014) Investigation on dissimilar underwater friction stir lap welding of 6061-T6 aluminum alloy to pure copper. Mater Des 64:74–80. https://doi.org/10.1016/j.matdes.2014.07.036
45. Mofid MA, Abdollah-zadeh A, Malek Ghaini F (2012) The effect of water cooling during dissimilar friction stir welding of Al alloy to Mg alloy. Mater Des 36:161–167. https://doi.org/10.1016/j.matdes.2011.11.004
46. Hui-jie L, Hui-jie Z, Huang Y-x, Lei YU (2010) Mechanical properties of underwater friction stir welded 2219 aluminum alloy. Trans Nonferrous Metals Soc China 20:1387–1391. https://doi.org/10.1016/S1003-6326(09)60309-5
47. Rai R, De A, Bhadeshia GKDH, Debroy T (2011) Review: friction stir welding tools. Sci Technol Weld Join 16(4):325–342. https://doi.org/10.1179/1362171811Y.0000000023
48. Zhang YN, Cao X, Larose S, Wanjara P (2012) Review of tools for friction stir welding and processing. Canadian Metallurgical Quarterly 51(3):250-261. https://doi.org/10.1179/1879139512Y.0000000015
49. Shanavas S, Edwin Raja Dhas J (2017) Parametric optimization of friction stir welding parameters of marine grade aluminium alloy using response surface methodology. Transactions of Nonferrous Metals of China 27:2334-2344. https://doi.org/10.1016/S1003-6326(17)60259-0
50. ASTM E8/E8M-09 (2010) Standard test methods for tension testing of metallic materials, ASTM International